ELSEVIER

Journal of Structural Geology 28 (2006) 588–601

JOURNAL OF STRUCTURAL GEOLOGY

www.elsevier.com/locate/jsg

The influence of water on deformation microstructures and textures in synthetic NaCl measured using EBSD

G.M. Pennock *, M.R. Drury, C.J. Peach, C.J. Spiers

Faculty of Geosciences, Utrecht University, Postbus 80.021, 3508 TA Utrecht, The Netherlands

Received 6 June 2005; received in revised form 25 January 2006; accepted 25 January 2006
Available online 23 March 2006

Abstract

Wet NaCl with >10–15 ppm water shows weakening behaviour compared with dry NaCl containing <5 ppm of water. At strains greater than about 0.1 this weakening is associated with recrystallization but at lower strains there is also considerable weakening that is thought to be associated with pressure solution creep. The development of textures and microstructures in wet, synthetic NaCl polycrystals deformed at elevated temperatures has been investigated using electron backscattered diffraction (EBSD). At very low natural strains (0.07), textures, grain shapes and average misorientations of subgrain boundaries in wet NaCl differ to those found in dry NaCl deformed under similar conditions. In wet NaCl, cube shaped grains, oriented in a hard orientation for slip on the ⟨110⟩{110} system, grow and produce a well defined sub texture, with ⟨100⟩ poles at 45° to the compression axis. An estimation of strain in wet NaCl was made using average misorientation values of subgrain boundaries. We estimate about 55% of the total strain was accommodated by dislocation creep in wet NaCl at 0.07 strain, the remaining strain being accommodated by pressure solution. At higher strains dynamic recrystallization occurs forming a ⟨100⟩ fibre texture. This texture can be explained by preferential nucleation of initially strain free grains, which occurs after a critical strain in the most highly deformed, soft-orientation grains, that is grains which have ⟨100⟩ parallel to the compression axis.

Keywords: Wet NaCl; Misorientation; Strain; Texture; Electron backscattered diffraction (EBSD)

1. Introduction

During plastic deformation at low temperatures (20–200 °C) and at laboratory strain rates, significant weakening is reported to occur in both natural and synthetic polycrystalline NaCl when intercrystalline brine is present (see Fig. 1) (Spiers et al., 1986; Urai et al., 1986; Peach et al., 2001). Above strains of about 0.1 weakening is associated primarily with dynamic recrystallization by enhanced fluid assisted grain boundary migration (Urai, 1983; Spiers et al., 1986; Ter Heege et al., 2005a). Only very little water, in excess of about 10–15 ppm, is needed to cause weakening (Watanabe and Peach, 2002; Ter Heege et al., 2005a): in such cases, the term wet NaCl is used here. The microscopic distribution of brine in polycrystalline NaCl is complex and has many important implications (see, for instance, Shenk and Urai (2004)). Under conditions of hydrostatic equilibrium, water is localized along grain boundaries and at triple junctions as isolated inclusions and tubes in accordance with dihedral angle considerations (Holness and Lewis, 1997). The pockets of water are thought to spread out into a thin film along grain boundaries during deformation due to dynamic wetting (Urai, 1983; Peach et al., 2001), increasing boundary diffusivity and enhancing grain boundary migration, which otherwise would not occur until temperatures above about 500 °C (Guillopé and Poirier, 1979; Franssen, 1993). Recent work shows that wetting of boundaries also occurs under static conditions when there is sufficient driving force for grain boundary migration (Shenk and Urai, 2004).

We use the term dynamic recrystallization to describe the growth of initially strain free grains that occurs in wet NaCl after a critical strain. Even at very low strains before the onset of widespread dynamic recrystallization, synthetic wet NaCl is 30–50% weaker than dry NaCl at strain rates of about $10^{-7}\,s^{-1}$. At these low strains, the microstructures of both materials contain subgrain boundaries (Watanabe and Peach, 2002) indicating that some strain was accommodated by dislocation creep. The weakening could be related to an effect of water on either dislocation creep or on the operation of enhanced intergranular deformation in the wet material.

* Corresponding author. Tel.: +31 30 2535109; fax: +31 30 2537725
E-mail address: gpennock@geo.uu.nl (G.M. Pennock).

0191-8141/$ - see front matter © 2006 Elsevier Ltd. All rights reserved.
doi:10.1016/j.jsg.2006.01.014

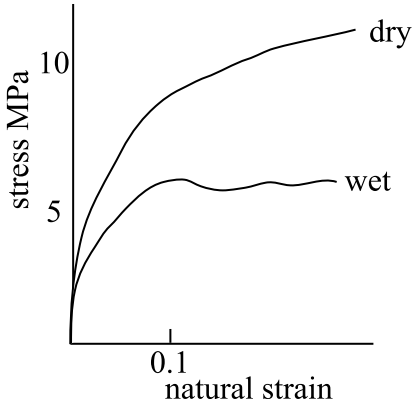

Fig. 1. Schematic diagram of stress versus strain for wet and dry polycrystalline NaCl deformed in compression, showing that wet NaCl is weaker than dry NaCl.

Calculations by Ter Heege (2002) suggest that at 0.07 strain up to 70% of the deformation could have been accommodated by fluid-enhanced grain boundary diffusion creep, or pressure solution (Spiers et al., 1990; De Meer et al., 2005). Though possibly coupled to pressure solution, grain boundary sliding is another possible mechanism that may also contribute to strain (Stokes, 1966).

Identifying active deformation mechanisms from microstructural signatures is a crucial step in obtaining mechanism-based rheological laws for geological materials (such as NaCl), which are suitable for extrapolation to natural conditions. In the absence of internal markers, identifying different deformation mechanisms from microstructures can be difficult (Passchier and Trouw, 1996), especially when more than one deformation mechanism operates. Diffusion creep can sometimes be recognised from segregation and overgrowth microstructures. In experimentally deformed material, grain boundary sliding can be inferred from split cylinder studies (Schmid et al., 1980), from internal marker particles in grains (Ree, 1994) and from the occurrence of diamond grain structures (Urai, 1987). In naturally deformed rocks grain boundary sliding is difficult to detect and possible indicators, such as a diamond grain structure, have been reviewed by White (1977), Drury and Humphreys (1988) and Ree (1994). Electron back scattered diffraction (EBSD) mapping is a particularly useful technique for determining changes in texture, microtexture and microstructure caused by dislocation creep (Randle, 1992; Humphreys et al., 2001) that occur in both naturally and experimentally deformed materials. Here the term microtexture means a population of orientations related to microstructure (Randle, 1992).

Trimby et al. (2000b) showed that misorientation angle distributions were significantly different for wet and dry NaCl at high strains because dynamic recrystallization removed subgrain boundaries in wet NaCl. In recent work on NaCl by Pennock et al. (2002) and Pennock and Drury (2005), EBSD mapping was used to determine the misorientation angle distributions of subgrain boundaries in dry NaCl as a function of strain. The average misorientation angle was found to be a useful parameter for describing the changes in the subgrain boundary misorientation distribution with strain (Hughes et al., 1997; Pennock et al., 2005); at low natural strains up to 0.5, a power law relationship was found to exist between strain and average misorientations of subgrain boundaries. These results indicate that, with suitable calibration, average subgrain boundary misorientations could offer a method for estimating the strain accommodated by dislocation creep in dry NaCl. Furthermore, if only limited grain boundary migration occurs, average misorientations could be used to estimate the strain accommodated by dislocation creep in wet NaCl during multi-mechanism deformation, providing there is no intragranular effect of water on dislocation mobility.

Textures (lattice preferred orientations) also differ in deformed dry and wet NaCl. Inverse pole figures (IPFs) of the compression axis show a maximum intensity in the ⟨110⟩ direction for dry NaCl 125–550° (Franssen and Spiers, 1990; Trimby et al., 2000b; Pennock et al., 2004) whereas in wet NaCl, at similar temperatures a ⟨100⟩ fibre texture occurs (Trimby et al., 2000b). In wet and dry NaCl at strains above about 0.1, this texture difference is caused by dynamic recrystallization, which occurs in wet NaCl, whereas a deformation texture is retained in dry NaCl (Trimby et al., 2000b). In a model, based on a self-consistent viscoplastic theory of polycrystalline plasticity, Wenk et al. (1997) and Lebensohn et al. (2003) investigated the effect of recrystallization and different deformation conditions in plastically anisotropic materials. The texture predictions for extrusive deformation using their model were in general agreement with textures observed in extruded NaCl, although the finite element methodology for averaging the polycrystalline response to deformation gave a better correlation to experimental data. The self consistent recrystallization model supports the idea that preferential nucleation occurs in grains that are more highly deformed (because they are in a soft orientation). In consequence, soft orientation grains commonly dominate recrystallization textures. Textures can be determined on a microstructural level using EBSD and used to test the current models of texture development.

Within the dislocation creep regime, nuclei for recrystallization in NaCl are most likely formed within highly deformed grains (Lebensohn et al., 2003). Subgrains are ubiquitous in NaCl deformed in the range of 125–500 °C and could be important nucleation sites for recrystallization (Humphreys and Hatherly, 1996; Humphreys, 2004). Subgrain boundaries in NaCl have widely varying misorientations and spatial distributions that vary with grain orientation and surrounding grain orientation (Trimby et al., 2000b; Pennock et al., 2005). Using EBSD, Pennock et al. (2002) and Pennock and Drury (2005) showed that individual subgrains in dry NaCl deformed at 165 °C were surrounded by segments of subgrain boundaries with a wide range of misorientations. Above strains of about 0.15, three types of subgrain boundaries were identified, depending on the boundary misorientation and distribution. Subgrain boundaries that surrounded equiaxed subgrains were ubiquitous at strains above about 0.15 and generally had lower misorientations ($<5°$), whereas extended subgrain boundaries rapidly developed higher misorientations even at low strains and were associated with triple points or dissected grains.

A weak core–mantle development of subgrains was also noted. In dry NaCl, some subgrain boundaries developed high misorientations, particularly at triple junctions (Pennock et al., 2004). The subgrain boundary types have not been studied in wet NaCl and knowledge of their distribution is needed to help identify possible locations for recrystallization.

The main purpose of this to study is to elucidate the effect that water has on the deformation mechanisms and textures in wet NaCl containing 28–68 ppm water. A point of particular interest was to determine the possible contribution of pressure solution in low strain deformation. Evidence for pressure solution at low strains might help to explain, for instance, recent work by Berést et al. (2005), which shows weakening, at very low strain rates, and flow stresses well below levels expected for dislocation creep. With this aim, microstructures and textures in wet deformed NaCl were determined using EBSD mapping and compared with those for dry NaCl (Pennock et al., 2005). Average misorientations of subgrains were used to estimate strain partitioning between dislocation creep and other mechanisms in wet NaCl.

2. Materials and methods

2.1. Sample preparation

Details of the deformation experiments and materials used in this work have been reported elsewhere (Peach and Spiers, 1996; Trimby et al., 2000a,b; Watanabe and Peach, 2002; Ter Heege et al., 2005a). Cylinders were prepared from synthetic NaCl by cold pressing and annealing to a final density of ~99.5% and water content of 37–290 ppm determined using whole sample Fourier transform infra red analysis. Initial average grain sizes were about 300 μm. The cylinders were deformed in axisymmetric compression using a triaxial testing machine under a confining pressure sufficient to inhibit dilatancy (Peach and Spiers, 1996), at constant displacement rate and temperatures ranging from room temperature to 165°C (Table 1). Typical stress–strain curves for the wet samples (p40t115, p40t112 and p40t92) showed work hardening to a peak stress at about 0.1 strain, followed by transient weakening and oscillatory stress behaviour (Watanabe and Peach, 2002; Ter Heege et al., 2005a) (shown schematically in Fig. 1). Final natural strains ranged from 0.07 to 0.18 in wet NaCl. Sample p40t115 (0.07 strain) was deformed to obtain work hardened microstructures before the initial stress drop and sample p40t112 (0.12 strain) to obtain microstructures at a low stress just after the initial stress drop. Sample p40t92 was deformed to a second, approximate peak stress occurring at higher strains (0.18). The dry samples showed continuous work hardening and higher flow strengths compared with wet samples at all strains (Table 1). Samples were sectioned soon after deformation to retain deformation microstructures. Sections were made of the central portion of the cylinder, parallel to the compression direction, and polished in a dry room (Urai et al., 1987). All sections were lightly etched for 10 s in saturated salt solution containing ferric chloride: etching was necessary to remove abrasive damage caused by polishing, thereby improving the analysis quality across low angle subgrain boundary misorientations.

2.2. Microscopy and EBSD

The microstructures were initially examined using light microscopy and orientation contrast imaging in the scanning electron microscopy (SEM). Conditions used for EBSD mapping NaCl were 12 kV accelerating voltage and about 2 nA beam current using a Philips XL30 SEM with a SIT camera, or a Philips XL30 SFEG SEM and a Nordlys CCD camera. EBSD data were collected and analysed using HKL Channel 5 software; typically 5–6 band centres were used to identify the patterns.

In order to map subgrain boundary misorientations and other substructures using EBSD, a step size of 4 μm was chosen, which was smaller than the average subgrain size. These small step maps were processed to improve the angular precision between adjacent pixels using VMAP (in-house software, courtesy of F.J. Humphreys, Manchester University). The angular precision of an SEM FEG system is about 1°

Table 1
Deformation information on wet and dry NaCl

Sample	References	Water (ppm)	Natural strain[a]	Confining pressure (MPa)	Strain rate (s^{-1})	Flow stress (MPa)	Deformation temperature (°C)	Grain size[b] (μm)
pk67		–	–	–	–	–	–	325±15
p40t115	Watanabe and Peach, 2002; Ter Heege et al., 2005a,b	32, wet	0.07 (b)	50	5×10^{-7}	11.1	125	305±15
pk119b	Pennock et al., 2005	7, dry	0.07	50	6×10^{-7}	11.2	165	330±13
p40t112	Watanabe and Peach, 2002; Ter Heege et al., 2005a,b	28, wet	0.12 (a)	50	5×10^{-7}	12.4	125	1026±60
p40t92	Trimby et al., 2000a,b	68, wet	0.18 (a)	50	5×10^{-7}	14.5	125	572±25
pk67m	Pennock and Drury, 2005; Pennock et al., 2005	6, dry	0.54	50	5×10^{-7}	15.1	165	139
pk73a	Pennock et al., 2005	11, dry	0.5	50	5×10^{-7}	14.6	165	117

[a] Samples before stress drop (b) and after stress drop (a).
[b] Grain sizes, expressed as an equivalent circle diameter, were determined from EBSD maps: >15° misorientation; ± shows the typical spread caused by ignoring grains with either 2 or 3 pixels.

(Humphreys et al., 2001; Pennock et al., 2002). Data processing involves averaging pixel orientations using a modified Kuwahara filter (Humphreys et al., 2001). This reduces many of the low misorientations caused by orientation noise and poor pattern quality along boundaries (Hurley and Humphreys, 2002). In the current work, two passes of a 3×3 filter enabled reliable detection of misorientations to better than 0.5° and gave a good representation of the etched microstructures (Pennock and Drury, 2005). Furthermore, average misorientation values could be compared with earlier work (Pennock et al., 2005).

EBSD large step mapping was used to examine grain shape microstructures and to determine textures and orientation gradients. In deformed NaCl, the average subgrain size was about 12 μm (Pennock et al., 2005) so a 40-μm-step accumulated misorientations across several subgrain boundaries and is a measure of the orientation gradient. Average orientation gradients determined from maps made from similar locations using different step sizes were found to be approximately linearly related to the average misorientations of individual subgrains (Pennock et al., 2002); therefore, trends in orientation gradient are expected to reflect trends in average subgrain misorientation. Individual subgrains were not imaged in large step maps but differences in their density and spatial distributions were apparent. EBSD mapped microstructures are presented with all non-indexed pixels replaced.

In order to assess textures, larger step maps of at least 100 grains were made (Table 2), which gave a reasonable evaluation of strong textures. For weak to almost random textures (e.g. p40t115), different areas within the EBSD map gave the appearance of a different texture (Pennock and Drury, 2005) and about 1000 grain orientations were needed to define bulk textures.

Some EBSD texture analyses of etched surfaces of NaCl have been reported as unreliable because of poor indexing (Lebensohn et al., 2003). The effect on textures of replacing non-indexed and misindexed pixels was therefore checked in this study. Automatic indexing of etched NaCl is generally not a problem with current software. In maps where the texture was extremely weak, replacing non-indexed pixels reduced the ⟨100⟩ pole density very slightly (p40t115), whereas the ⟨001⟩ pole density strengthened very slightly in a map containing a single, poorly indexed grain (p40t92). If poor indexing of an order of 10% remains in EBSD maps, textures can be slightly influenced if only a few grains are mapped or if the texture is weak. In maps in which the number of grains was greater than 100 and/or the texture was strong, processing made no significant difference to the textures.

3. Results

3.1. Microstructures

Microstructures examined using light microscopy have been presented elsewhere (Peach and Spiers, 1996; Watanabe and Peach, 2002; Ter Heege et al., 2005a). For completeness, these results are summarised here. Grains in undeformed synthetic wet NaCl were equiaxed with almost no internal substructure and arrays of brine were present along grain boundaries. Some intra-granular brine inclusions were also observed (Watanabe and Peach, 2002). Little change was observed in the grain shape and size after 0.07 strain (pk119b and p40t115), although in wet samples many grain boundary traces were aligned at about 45° to the compression axis. The amount of substructure varied from grain to grain at 0.07 strain in both wet and dry material; some grains contained long etch features, others contained distinct subgrains, while other grains showed little or no substructure, particularly in the wet sample. In the wet sample deformed to 0.07 strain, subgrains tended to be located predominantly near grain boundaries of larger grains At higher strains, just beyond the first stress peak, wet deformed sample p40t112 was partially recrystallized, which caused a large increase in grain size (Table 1).

Moving to the EBSD results, an overview of the changes occurring in the grain scale microstructures in undeformed as well as wet and dry low strain material are illustrated in Fig. 2. Grain boundaries are shown as black lines at locations where the misorientation between pixels was greater than 15°. Clear differences are apparent in the grain shapes and sizes. Undeformed NaCl contained mostly polygonal grains with the occasional cube shaped grain (Fig. 2a). Some undeformed samples contained a few large grains that enclosed smaller, internal grains. The size and shape of grains after 0.07 strain in the dry sample (Fig. 2b) was similar to the undeformed sample. The grain size of the wet sample deformed to 0.07 strain (Fig. 2c) was similar to the undeformed material, but inspection

Table 2
EBSD step sizes and textures

Sample (strain, water)	Step size (μm)	Number of grains	Maxima in IPF of compression axis	Intensity IPF[a]	
				Minimum	Maximum
pk67 (undeformed)	40	1067	weak 110	0.9	1.1
pk119b (0.07, dry)	40	930	110–weak 115	0.7	1.2
p40t115 (0.07, wet)	40	1491	Weak 110	0.9	1.1
Cube shaped grains			111 maxima	0.5	1.61
Irregularly shaped grains			001 maxima	0.7	1.1
p40t112 (0.12, wet)	40	101	001	0.4	2.2
p40t92 (0.18, wet)	25	165	Close 001	0.3	2.5
pk67m (0.54, dry)	40	>>1000	110–weak 115	0.2	1.9

[a] Multiples of random density.

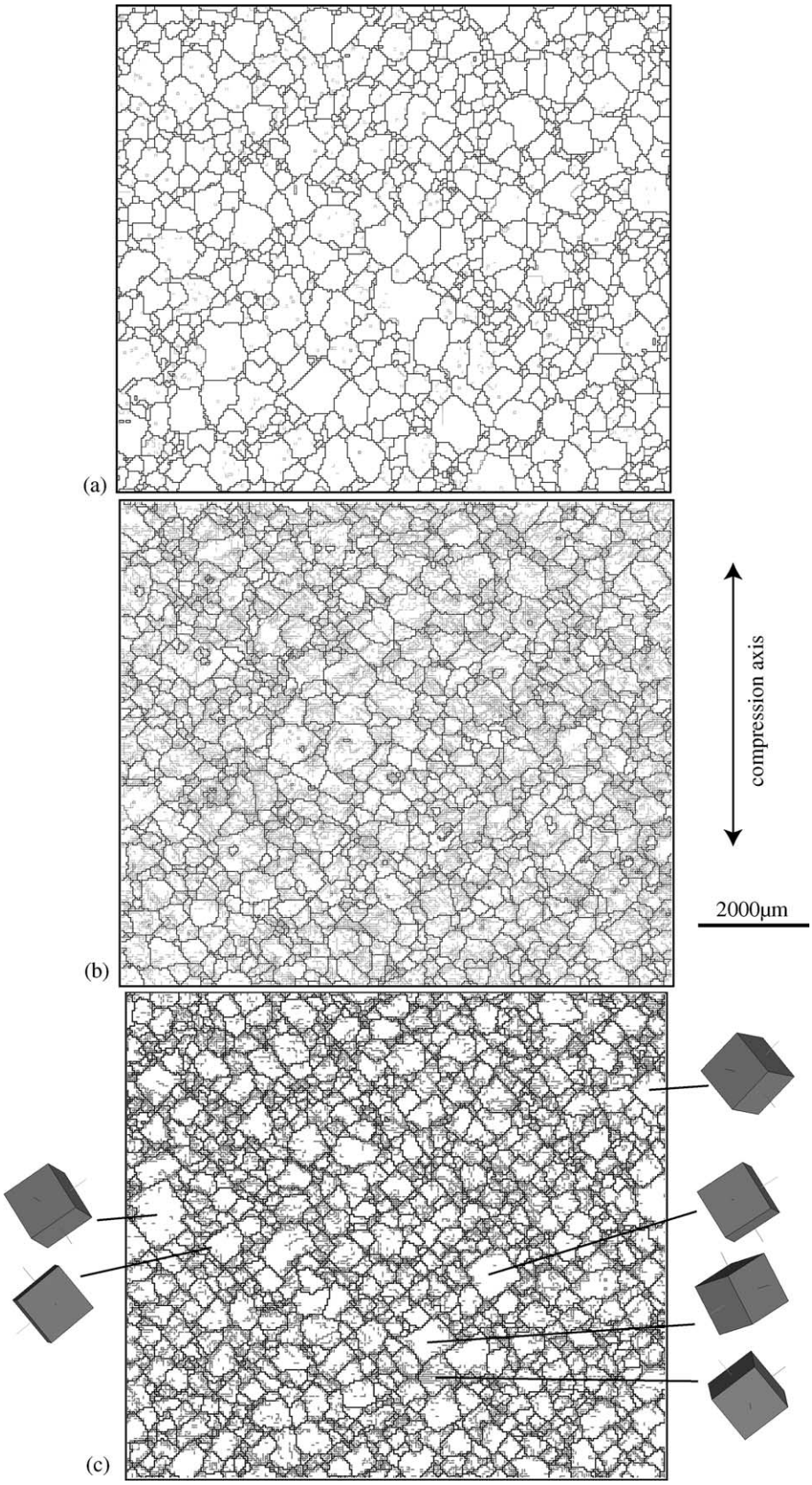

Fig. 2. Grain shapes and substructure in (a) undeformed (pk67) and (b) and (c) 0.07 strained dry (pk119) and wet (p40t115), respectively. The wet deformed sample contains more cube shaped grains than the undeformed and dry samples. More subgrains are present in the dry deformed sample than in the wet deformed sample. The crystal orientation of several cube shaped grains is shown schematically as cubes. (40 μm step mapping, grain boundaries are shown as black lines and subgrain boundaries with misorientations $>1.3°$ as grey lines.)

of Fig. 2 shows that wet NaCl microstructures contained more square sectioned grains, cube shaped in 3D, than either the undeformed material or dry samples deformed to the same strain. Furthermore, the 45° alignment of grain boundaries in the wet sample was related to the preferential alignment of the faces of cube shaped grains (Fig. 2c). Comparison of the crystal orientation of the cube shaped grains (schematically represented as cubes) with the grain boundary traces shows that many of the grain boundaries traces were subparallel to {100} crystal faces. Corners of cube shaped grains occasionally jutted out into a neighbouring grain and did not form a triple junction. Within the same wet sample (p40t115) cube shaped grains had a larger average grain size than irregularly shaped grains (Table 3).

Misorientations in the range from 1.5° to <15° are shown in Fig. 2 as grey lines. Whereas the undeformed microstructure contained only a few subgrain boundaries (Fig. 2a), subgrains in the dry deformed sample (Fig. 2b) were relatively widespread throughout all grains, although the density varied from grain to grain. Fewer subgrains were present in the wet sample deformed to the same strain (Fig. 2c) and these tended to be located near to grain boundaries.

A more detailed EBSD mapped microstructure of the grain shapes and substructure in deformed wet and dry NaCl is shown in Fig. 3 after 0.07 strain. At these very low strains, the mapped microstructures were similar to the etched microstructures, but some very low angle subgrain misorientations are below the angular resolution for EBSD (Pennock et al., 2005). The long etch features observed in light microscopy were identified as extended subgrain boundaries with sections having misorientations of 4–5°. Several grains show a slightly higher density of subgrains occurring in the boundary region compared with the core of the grain and a few grains show equiaxed subgrains. Similar to the light microscopy results, fewer subgrain boundaries were observed in the EBSD maps of the wet NaCl compared with the dry NaCl after 0.07 strain. Even at such low strains (<0.1), deformation of wet NaCl caused limited grain boundary migration in the form of small bulges, particularly at or near triple junctions but also occasionally along grain boundaries. Triple junction bulges formed along boundaries at all angles to the compression axis. Many of the bulged regions contained similar levels of subgrains compared with the parent grain, although often a higher misorientation subgrain boundary occurred between a bulge and the parent grain in line with the original grain boundary (Fig. 4). Bulging along the grain boundary occurred in only a few grains at 0.07 strain in wet NaCl and was not as common as bulging at triple junctions. Bulging along grain boundaries was more common at higher strains (>0.1).

In wet samples deformed just beyond the stress drop, to 0.12 strain (Fig. 5), dynamic recrystallization occurred causing an increase in grain size (Table 1). The majority of the grains were irregularly shaped, although a few cube shaped grains were also present. The crystal orientations of several cube shaped grains shows that many of grain boundaries traces were parallel to {100} crystal faces. However, the alignment of the cube shaped grains in material deformed beyond the stress drop was more random than in samples deformed to only 0.07 strain, where most boundaries were aligned at $45 \pm 10°$ to the compression axis.

3.2. Average misorientation angles

Frequency distributions of orientation gradients across several subgrain boundaries are shown in Fig. 6. In undeformed material, orientation gradient distributions, measured using a 40 μm step, predominantly caused by angular resolution limits of the EBSD system, peaked at about 0.4°. In deformed materials, the frequency distributions of orientation gradients shifted to angles above the angular resolution limit of EBSD. Dry NaCl deformed to 0.07 strain showed slightly higher orientation gradients compared with the wet NaCl deformed to the same strain: average orientation gradient values were, respectively, 1.68 and 1.23°/40 μm (standard error, 90% confidence limit determined for 40 grains was ±0.07°/40 μm: standard errors for complete maps are expected to be less, as more grains were averaged).

Cube shaped grains were manually selected as a subset in mapped microstructures of the wet sample deformed to 0.07 (p40t115). As mapping with a large step tends to simplify grain shapes, selection of cube shaped grains was also made on the basis of grains having 3–4 rectilinear boundaries in orientation contrast images. The frequency distribution of the orientation gradients (Fig. 6b) for cube shaped grains differed to irregularly shaped grains, with the cube shaped grains showing a higher frequency of lower orientation gradients. Average orientation gradients differed by 0.46°/40 μm less in the cube shaped grains (Table 3).

Smaller step (4 μm) mapping provided direct information about average misorientations across individual subgrain

Table 3
Properties of cube and irregularly shaped grains (p40t115, wet, 0.07 strain, EBSD 40 μm step)

Selection	Average grain size (μm)	Number of grains (% mapped area)	Average orientation gradient (<16°, °/40 μm)	Intensity {100}[a]	
				Minimum	Maximum
Irregularly shaped grains	282[b]	1284 (72)	1.54	0.6	1.3
Cube shaped grains[c]	484	188 (25)	1.08	0.1	2.6
Complete map	305[b]	1409 (98)	1.23	0.7	1.2

[a] Multiples of random density.
[b] Only grains >3 pixels.
[c] Grains selected on basis of forescatter images.

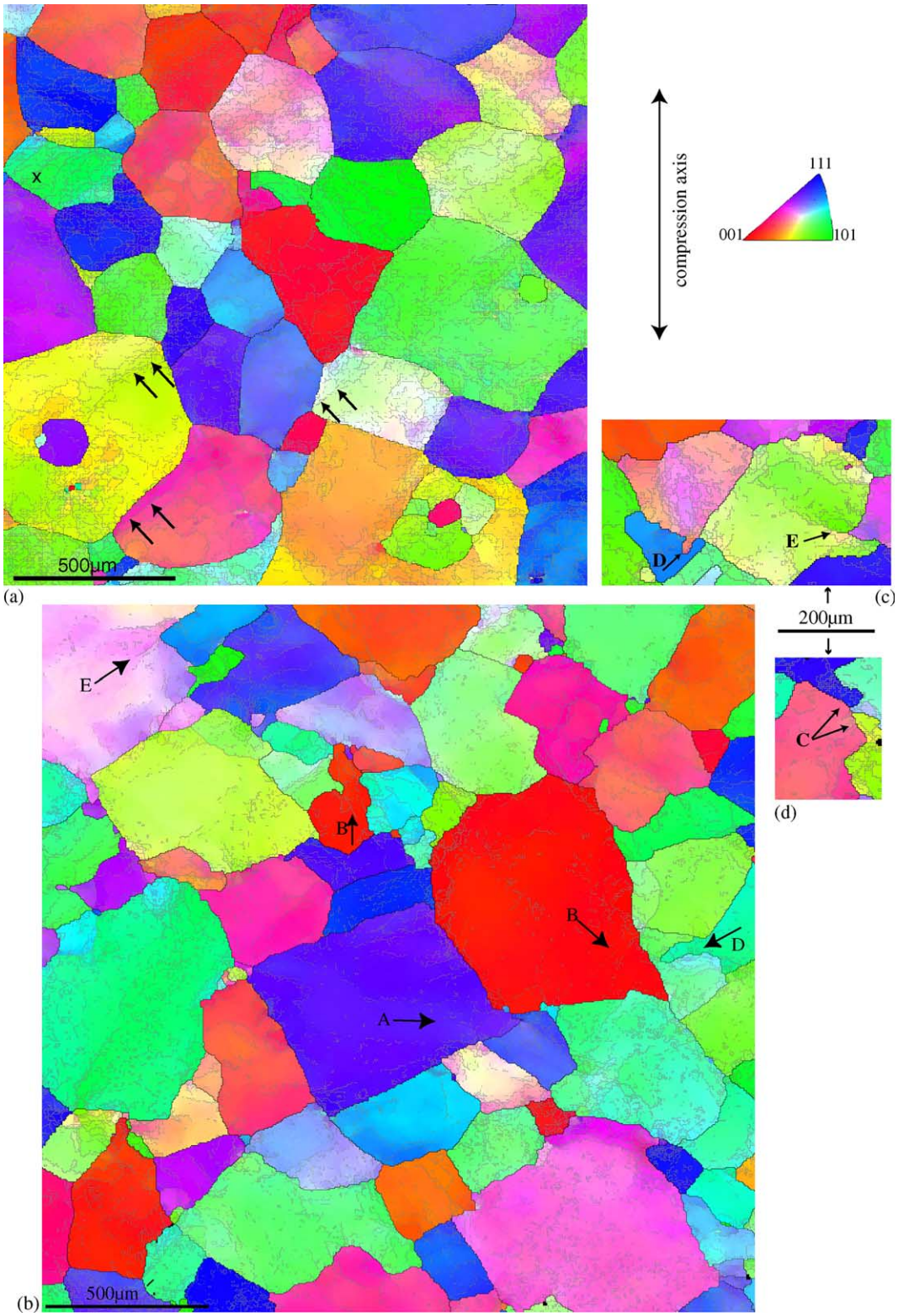

Fig. 3. Detailed microstructures of grain shapes in (a) dry and (b)–(d) wet NaCl, deformed to 0.07 strain. (a) Grain shapes are similar to undeformed material and only a few cube shaped grains are present: equiaxed subgrains are shown in grains X, and three extended subgrain boundaries are shown with arrows. (b)–(d) Many more cube shaped grains are present compared with the dry deformed material. Many corners of cube shaped grains are not associated with a triple junction. Extensive triple junction grain boundary migration occurs. Bulging at triple junctions of cube (A) and irregularly (B) shaped grains is common. Triple junctions mostly migrate along existing grain boundaries, sometimes in opposite directions along the same grain boundary (C). Occasionally the triple junction does not migrate with the bulge and the grain forms a peninsular into the neighbouring grain (D). High misorientation subgrains often form ahead of peninsular bulges and corners of cube shaped grains that do not form at triple junctions (E). (4 μm step mapping, subgrain boundaries with misorientations $>0.5°$ are shown as grey lines and grain boundaries with $>10°$ misorientation are shown as black lines.)

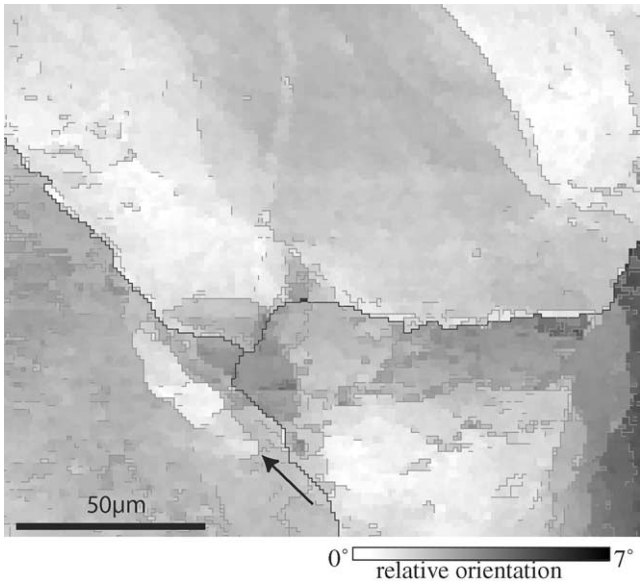

Fig. 4. Detail of subgrain boundaries at a triple junction. Subgrain boundaries occur below a bulge and in line with the grain boundary (arrowed). (Wet NaCl, 0.07 strain, subgrain boundaries $>0.7°$ shown as grey lines, grain boundaries $>10°$ shown as black lines, 1 μm step mapping.)

boundaries at low strains. At low strain (0.07) the average misorientation from 4 μm mapping of the wet material was lower than that found in dry material. For wet NaCl, the average misorientation value, θ_{av}, was found to be 1.01° compared with a value of 1.33° for the dry NaCl ($\pm 0.04°$ standard error to 90% confidence based on averages for about 100 grains (Pennock and Drury, 2005)).

3.3. Textures

IPFs are shown in Fig. 7 and corresponding details are summarized in Tables 2 and 3. The IPFs show the compression axis and completely describe the textures (Skrotzki and Welch, 1983). Differences in texture for the 0.07 low strained samples are highlighted using pole figures.

The undeformed material (sample pk67) showed an almost random texture, with a very slight alignment of the ⟨110⟩ poles parallel to the compression axis. At 0.07 strain (pk119b), in dry NaCl, the ⟨110⟩ maximum increased slightly, with some spreading of poles towards ⟨115⟩. The ⟨110⟩ maxima for the dry sample at 0.07 strain was stronger than the wet sample (p40t115) deformed to the same strain. Microtextures of cube and irregularly shaped grains in the wet sample showed ⟨111⟩ and ⟨001⟩ maxima, respectively, with some spread towards ⟨110⟩ for both types of grain. After the stress drop, at 0.12 strain (sample p40t112), the fully recrystallized wet material developed a ⟨100⟩ fibre texture, which was strengthened at higher strains (0.18; sample p40t92) (Trimby et al., 2000b). In contrast, deformation of dry NaCl to high strains of 0.54 (sample pk67m) maintained a ⟨110⟩ fibre texture.

The {100} pole figures for the wet and the dry NaCl deformed to 0.07 strain also differed. The {100} poles of the dry sample tended to form incomplete girdles, one at about 10° to the compression axis and a second girdle perpendicular to the compression axis, whereas for the wet sample the {100} poles tended to be at 45° to the compression axis. Microtextures of cube and irregularly shaped grains showed that the bulk texture of the wet sample was comprised of two distinct textures. Cube shaped grains had {100} poles aligned along girdles at 45° to the compression axis. The remaining irregularly shaped grains showed a maximum of {100} parallel to the compression axis. The {111} poles showed complimentary alignments, with {111} showing a maximum sub-parallel to the compression axis in the wet material. These trends are also apparent by the blue colouring of many of the cube shaped grains shown in Fig. 4b. For the higher strain samples (P40t112; 0.12 strain), only a few cube shaped grains were mapped but their texture was similar to the bulk texture with {100} poles aligned parallel to the compression axis.

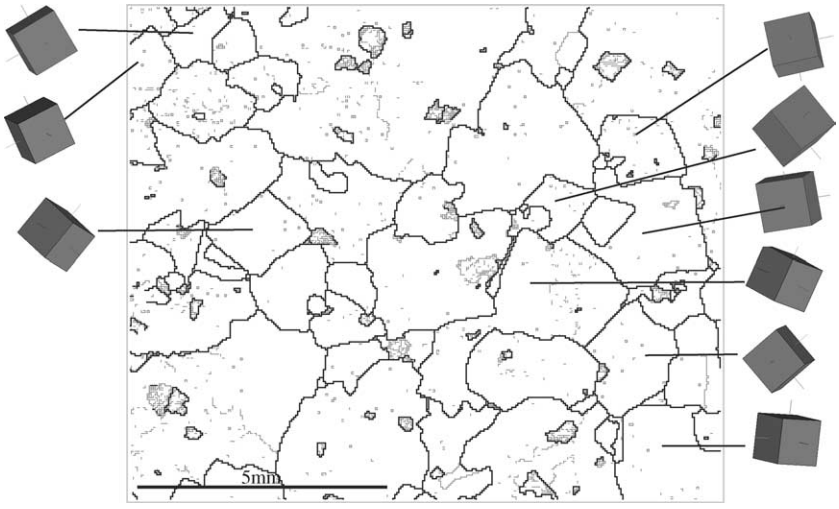

Fig. 5. EBSD mapped microstructures of dynamically recrystallized wet NaCl after the stress drop (sample p40t112, strain 0.12) showing cube (about 19% of the mapped area) and irregularly shaped grains, remnant grains and subgrain boundaries. The crystal orientation of several cube shaped grains is shown schematically as cubes. (40 μm step mapping, grain boundaries are shown as thick black lines and subgrain boundaries with misorientations $>1.3°$ as grey lines.)

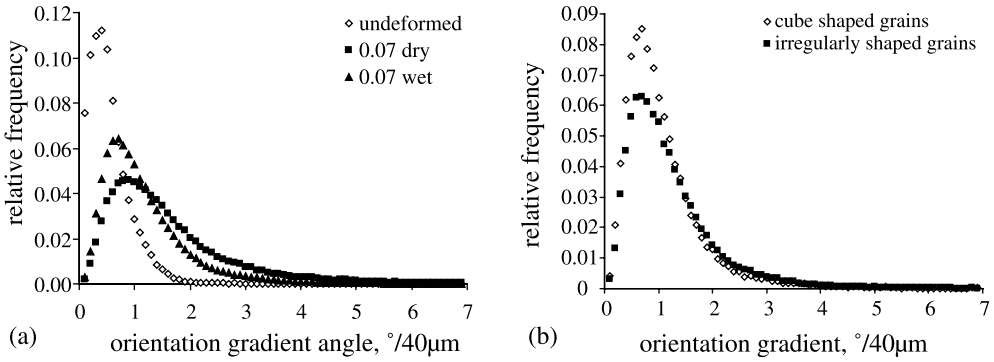

Fig. 6. Low angle frequency distribution of orientation gradients: (a) undeformed material and material after 0.07 strain. In deformed material, the frequency distribution is shifted to higher angles because of the presence of subgrain boundaries. Orientation gradients are higher in the dry deformed NaCl material compared with the wet deformed material. (b) Irregularly shaped grains show slightly higher orientation gradients compared with the cube shaped grains (40 μm step mapping).

3.4. Schmid factors

Fig. 8 shows the Schmid factors for slip on {110} ⟨101⟩ for cube and irregularly shaped grains in wet NaCl deformed to 0.07 strain. The cube shaped grains generally had a lower frequency of high Schmid factor values for this slip system compared with irregularly shaped grains, indicating that slip was relatively harder in the cube shaped grains. Schmid factors for the {100} ⟨011⟩ slip system showed similar frequency distributions for both cube and irregularly shaped grains. Similar trends were observed in all wet deformed samples.

4. Discussion

Wet synthetic NaCl is weaker than dry NaCl, even at very low strains before dynamic recrystallization occurs. At both low and high strains, EBSD microstructures and textures clearly show differences between wet and dry NaCl in terms of the subgrain misorientations, the textures and the shape and size of grains. These changes are discussed in terms of low then high strain behaviour.

4.1. Low strain (<0.1) behaviour

The amount of dislocation creep was demonstrably less in wet NaCl compared with that occurring in dry NaCl deformed to the same strain. This is shown by the slightly weaker textures and the lower average misorientation value found for the wet NaCl. The differences in both texture and average misorientation were associated with the cube shaped grains present in wet NaCl. Although the bulk texture of the low strained wet sample was weak, the microtexture of the cube shaped grains, which was based on 188 grains, was quite strong.

Significantly, the cube shaped grains increased in number and size in the wet NaCl compared with dry material deformed to the same strain. These grains showed a tendency for their ⟨111⟩ and ⟨110⟩ poles to be parallel to the compression axis. Slip in NaCl occurs primarily on the {110} ⟨101⟩ system, although slip on {100} ⟨101⟩ can also occur at higher temperatures (Skrotzki, 1994). The ease with which a grain deforms depends on its orientation with respect to the deformation axis and can be described in terms of the Schmid factor: a high Schmid factor (maximum of 0.5) (Hull and Bacon, 1984) indicates that slip is easy. Grains oriented with their ⟨110⟩ to ⟨111⟩ parallel to the compression axis are in a harder orientation for slip on the {110}⟨101⟩ slip system than ⟨100⟩ oriented grains. The grains in the harder orientation should therefore deform less than grains in a soft orientation (Lebensohn et al., 2003). This is supported by the lower orientation gradients and lower Schmid factor values of cube shaped grains compared with the irregularly shaped grains in the wet sample. As the strain was quite low in the wet sample and, according to the average orientation gradient values, concentrated more in the irregularly shaped grains, then the likelihood is that the cube shaped grains have a virtually unchanged orientation compared with their original, undeformed state. It is therefore likely that the bulk texture changes in the wet NaCl sample are associated with the observed increase in grain size of the cube shaped grains. In the present samples, preferential growth at low strains probably occurred as a means of lowering stored energy differences between the hard, less deformed grains and the softer grains, in agreement with thte recrystallization model of Wenk et al. (1997). Growth of the hard grains, which developed into cube shapes, most likely involved fluid assisted grain boundary migration (Spiers et al., 1986; Peach et al., 2001), because high temperatures (>500 °C) are needed for grain boundary migration of dry NaCl (Guillopé and Poirier, 1979; Franssen, 1993).

The alignment of the grain faces of cube shaped grains parallel to the {100} crystallographic planes suggest that their shape was determined by anisotropic growth rates. The {100} cube face of NaCl have the lowest surface energy and are close packed faces (Read and Watson, 1969). The alignment of the {100} cube faces at 45° to the compression axis therefore seems to be a secondary effect and is most likely a consequence of preferred growth of hard grains, which have a greater tendency to be oriented with ⟨110⟩ to ⟨111⟩ parallel to the compression axis (Fig. 7j), coupled with anisotropic growth of the grains. The presence of grain boundaries at 45° to the compression axis would favour subsequent grain boundary sliding, as suggested by microstructures (Fig. 5) that show high

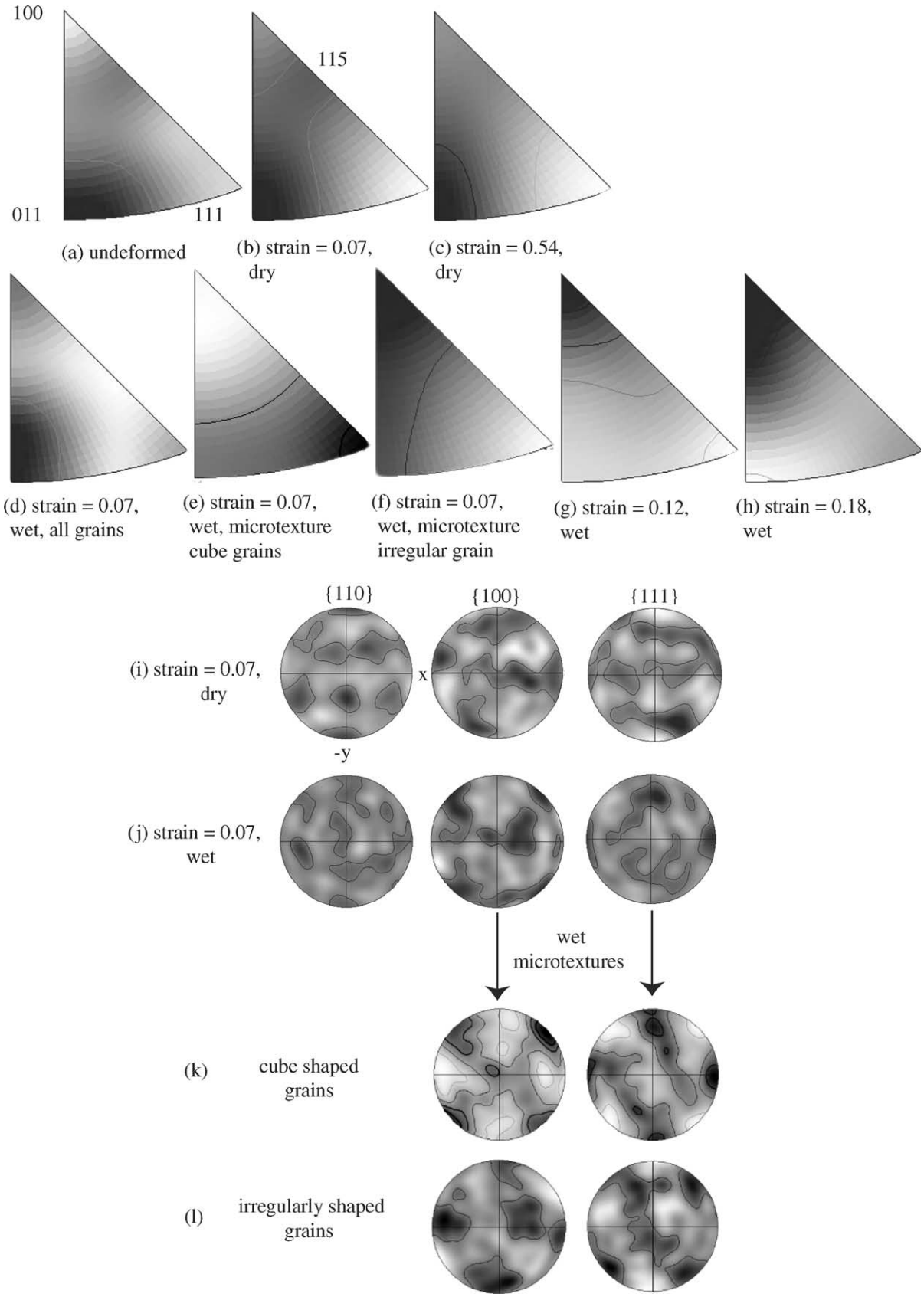

Fig. 7. Textures of deformed wet and dry NaCl deformed in compression: (a)–(h) IPFs of the compression axis and (i)–(l) IPFs of the major fibre textures after 0.07 strain (*y*-axis parallel to the compression axis). Microtextures are shown for wet NaCl for cube shaped grains ((e) and (k)) and irregular shaped grains ((f) and (l)) (contoured with a half width of 20° in 0.5 multiples of random density).

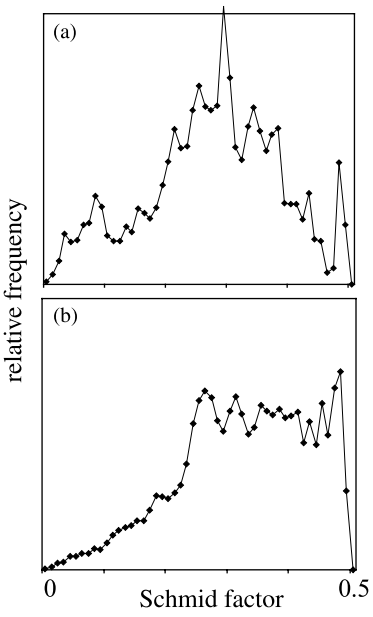

Fig. 8. Relative frequency of Schmid factor for {110} ⟨101⟩ slip in (a) cube shaped and (b) other shaped grains. Cube grains show a lower frequency of high Schmid Factor values indicating that slip is relatively harder in these grains. (40 μm step, EBSD map, 0.07 strain, wet NaCl.)

misorientation subgrain boundaries behind bulges and in-line with the grain boundary trace.

Grain boundary alignments at 45° to the compression axis (or foliation plane in naturally deformed rocks) have been observed in metals and minerals (Singh et al., 1973; Lister and Dornsiepen, 1982; Urai, 1987; Drury and Humphreys, 1988; Ashton and Humphreys, 2004). These alignments are thought to form by a process involving sliding along grain boundaries, which creates localized deformation zones ahead of triple junctions that subsequently migrate (Type M structure (Drury and Humphreys, 1988)). This mechanism does not seem to be involved in the preferential migration of triple junctions boundaries found in wet NaCl, as localized boundary migration at triple junctions occurred in irregularly shaped grains as well as cube shaped grains and sliding along the curved boundaries of irregular shaped grains would not be transmitted to the triple junction. Furthermore, migration of triple junctions occurred at all angles to the compression axis and, in one case, in opposite directions along the same grain boundary. In the grain boundary sliding related mechanism (Type M), the direction of grain boundary migration is ahead of the grain boundary with a high shear stress. The microstructures observed in the wet NaCl at low stress are not consistent with grain boundary migration ahead of a sliding boundary. Strain gradients may also develop within individual grains during deformation in order to accommodate inhomogeneous strain between adjacent grains (Ashby, 1970) and these strain gradients tend to be localized in grain boundary regions and near triple junctions, as evidenced by the formation of high misorientation, extended, subgrain boundaries in the vicinity of triple junctions in both wet (Fig. 4) and dry NaCl (Pennock and Drury, 2005). Localized triple junction migration along extended subgrain boundaries would reduce strain energy and result in the formation of peninsular grains. Other triple junction geometries, in which the triple junction migrates along the grain boundary, suggests that migration occurs either to remove higher strain energy regions next to the boundary, or to remove higher interface energy boundaries. In all cases, migration would be enhanced by water pockets located at triple junctions (Peach et al., 2001).

The presence of a 'diamond grain microstructure' is often invoked as evidence for grain boundary sliding, or grain boundary sliding in combination with grain boundary migration (Types N and M, respectively (Drury and Humphreys, 1988)). The current work shows that another mechanism of preferential anisotropic growth in cubic materials may also cause alignment of {100} grain boundaries at 45° to the compression axis, thereby creating a diamond grain microstructure. This type of diamond grain structure, which can be termed a Type G structure, indicating a growth controlled mechanism is operative, does not require any grain boundary sliding to form, although, once the alignment has occurred, the boundaries are in the ideal orientation for sliding. The mechanisms involved in the formation of a diamond grain structure therefore need to be investigated before the structure can be used as an indicator of grain boundary sliding. Careful analysis of the lattice preferred orientation together with microstructural analysis is a needed to distinguish between the different types of structure.

Turning to our data on average subgrain boundary misorientations (θ_{av}), at low strains, the power law relationship for dislocation creep in dry NaCl, $\theta_{av}=k\varepsilon^n$, where ε is strain, $k=4.1°$ and $n=0.43$ (Pennock et al., 2005), can be used to obtain an estimation of the strain caused by dislocation creep in the wet material. This strain contribution was calculated to be 0.039, which is $55\pm5\%$ of the measured strain value of 0.07. Similar strain estimates for dislocation creep (0.04) were also determined from the average orientation gradients based on 40 μm step mapping. This application of an average misorientation strain relationship derived from dry NaCl to wet NaCl requires some justification. At very low strains before any softening occurs, the misorientation angle and spatial distributions of subgrain boundaries in wet deformed NaCl are very similar to those found in dry NaCl, implying that the essential processes of slip and recovery in the two materials were similar. In silicates and alumina, 'water weakening' occurs (Mackwell et al., 1985; McLaren et al., 1989; Kronenberg et al., 2000) by processes that influence dislocation mobility (Carter et al., 1990). In quartz, this hydrolytic weakening effect is believed to be related to hydration of the Si–O bond (Mackwell et al., 1985). It is important to note that water weakening is not strong in all minerals. In calcite, for example, water does not affect the dominant mechanism of dislocation recovery or creep (Rutter, 1972; De Bresser et al., 2005). Rinsing in undersaturated solution or pure water can dramatically enhance ductility of single crystals of NaCl (Joffe effect) but the exact mechanism involved is almost certainly related to surface dissolution and precipitation effects (Martin et al., 1999) and should not be taken as evidence for an interagranular effect. To date, there is no firm evidence that

intracrystalline water, or water related species, affect slip or climb in NaCl (Carter et al., 1990; Watanabe and Peach, 2002), or even dissolve measurably in the NaCl lattice. However, there is an abundance of evidence that weakening of NaCl can be accounted for in terms of pressure solution, without evoking any effect of water on dislocation mobility (Urai et al., 1986; Spiers et al., 1990; Spiers and Brzesowsky, 1993; Peach et al., 2001; Ter Heege et al., 2005b).

Average subgrain misorientation values may also be influenced by grain size and stress (Pennock et al., 2005): in the wet NaCl, the bulk stresses of the wet and dry samples deformed to 0.07 strain were very similar because of differences in test temperature (Table 1), so stress differences cannot influence the average misorientation values of these two samples. In the absence of dynamic recrystallization, which removes subgrain boundaries (Trimby et al., 2000b), temperature is not expected to influence directly the average misorientations. Although the average grain size of the cube shaped grains was slightly larger than the irregularly shaped grains, the average grain size of the whole microstructure was similar to the dry NaCl, so grain size is not expected to influence the lower average misorientations of the wet NaCl compared with the dry for the complete data set. As localized grain boundary migration occurred even at very low strains in the wet NaCl at both triple junctions and in cube shaped grains, dislocation creep strain in wet NaCl may be slightly underestimated using the average misorientation–strain relationship for dry NaCl. However, the localised regions were small ($\sim$2% of the mapped area in Fig. 4b) and contained subgrains, so the effect is expected to be small. An inhomogeneous distribution of subgrains (Pennock and Drury, 2005), however, may cause a slight overestimate of the dislocation creep strain.

The estimate of 50–60% dislocation creep strain based on average misorientation measurements for our wet sample deformed to 0.07 strain compares favourably with an estimate of strain partitioning into 35–70% pressure solution strain and 30–65% dislocation creep by Ter Heege et al. (2002, 2005a) on the same sample. Both independent estimates suggest an important role for pressure solution creep accommodating 35–70% of the imposed strain. Pressure solution may accordingly be responsible for the enhanced deformation rates, with respect to extrapolated dislocation creep flow laws, observed in low strain experiments at very low stresses (Bérest et al., 2005), in cavity convergence measurements (Campos de Orellana, 1998) and in enhanced subsidence rates over deep solution mining cavities in North Netherlands (Breunese et al., 2003). Better correlation was found between measured subsidence and convergence rates using the pressure solution flow law of Spiers et al. (1990) to the relevant conditions (Campos de Orellana, 1998; Breunese et al., 2003).

4.2. Higher strain (>0.1) behaviour

The limited growth of the hard grains only occurred at low strains in wet NaCl: after the stress drop, extensive dynamic recrystallization occurred (Drury and Urai, 1990). Although the initial microstructure favoured grain growth of the hard grains with ⟨110⟩ to ⟨111⟩ subparallel to the compression axis to form cube shaped grains, these grains were replaced at higher strains. Larger, mainly irregularly shaped grains, with a dominant ⟨100⟩ texture component, replaced both the cube shaped grains and the bulk ⟨110⟩ fibre texture formed by dislocation creep. The change in recrystallization texture, the oscillatory stress–strain curves and the growth of relatively strain free grains all suggest that dynamic recrystallization is controlled by a nucleation event. The change in texture can be explained by the model of Wenk et al. (1997) in which preferential nucleation occurs in the more highly deformed, soft oriented, ⟨100⟩ grains after a critical amount of strain. In metals, oscillatory stress–strain behaviour occurs when discontinuous dynamic recrystallization results in an increase of grain size (Sakai and Jonas, 1984). In general, the nucleation site is difficult to identify (Humphreys, 2004). We have not studied wet NaCl material at the peak stress, that is at the strain at which new grains are expected to develop, so we have no definite evidence for a nucleation site. We have only observed microstructures after the stress peak, in which extensive growth of relatively strain free grains has occurred. Work on dry NaCl (Trimby et al., 2000b; Pennock et al., 2004) has shown that small, new grains, or high angle subgrain boundaries, form at triple junctions at strains of about 0.3–0.5. These new grains have a ⟨100⟩ orientation parallel to the compression axis (Pennock et al., 2004), so they could act as nuclei in the wet recrystallized NaCl, but the strains at which the new grains form in dry NaCl is much higher than the strains at which recrystallization occurs in wet NaCl. Furthermore, localized migration at triple junctions occurs at very low strains of about 0.1 in wet NaCl, which would tend to remove any high misorientation boundaries that may form at triple junctions. The actual mechanism involved in nucleation of dynamic recrystallization in wet NaCl therefore remains unclear. Another explanation for the change in texture might be oriented growth of ⟨100⟩ grains but at low strains these grains have higher stored energy than harder grains. For oriented growth to occur at high strains some process is needed to reverse the stored energy differences between hard and soft grains observed at low strains. Further microstructural analysis is needed just before the onset of dynamic recrystallization to determine the details of the nucleation process.

In summary, our work has shown that three regimes of deformation and texture development can occur in NaCl: dry deformation behaviour and low and high strain wet deformation behaviour. In wet NaCl, the development of a distinctive texture (Fig. 7k) is an interesting new finding. The texture in this regime is produced by preferential growth of hard grains under conditions where deformation occurs by a combination of dislocation creep, fluid assisted grain boundary migration and pressure solution. As there is significant pressure solution, migration of boundaries must be accompanied by mass transfer along boundaries and around grain surfaces (Ree, 1994; Shenk and Urai, 2004). The microtextures of cube and irregularly shaped grains formed in wet NaCl at low strains differs from the ⟨110⟩ fibre texture formed by dislocation creep

in dry NaCl and the ⟨100⟩ fibre texture caused by dynamic grain boundary recrystallization that dominates high strain wet NaCl.

5. Conclusions

1. EBSD mapping of wet NaCl microstructures and textures shows clear differences compared with dry deformed NaCl, even at very low compressive strains before the stress drop at a strain of 0.1.
2. In wet NaCl subject to axial compression, grains in a hard orientation for slip increase in grain size and develop cube shapes at low strains (<0.1). These grains develop a strong texture with ⟨100⟩ cube directions at $\pm 45°$ to the compression axis. This texture is distinct from the weak ⟨110⟩ fibre texture that develops in dry NaCl.
3. At axial compressive strains >0.1, extensive dynamic recrystallization occurs. A ⟨100⟩ fibre texture develops, which can be explained by preferential nucleation in the soft orientated grains.
4. Based on the average misorientation value of subgrain boundaries, dislocation creep strain was estimated to accommodate 50–60% of the bulk strain in wet NaCl strained to 0.07. The remainder is likely to be pressure solution.

Acknowledgements

Pat Trimby is thanked for providing the EBSD map data for one of the samples. Sandra Piazolo and Janos Urai are thanked for their reviews and comments that have helped to improve this paper. Peter van Krieken is thanked for carrying out some of the deformation experiments and Jaap Liezenberg for sample preparation. The electron microscopy was conducted at the Utrecht University Electron Microscopy Unit (EMU).

References

Ashby, M.F., 1970. The deformation of plastically non-homogeneous materials. Philosophical Magazine 21, 399–424.

Ashton, M.J., Humphreys, F.J., 2004. Inhomogeneous deformation and microstructural evolution during hot deformation of Al–4.98Mg. Material Science Forum 467–470, 117–122.

Bérest, P., Blum, P.A., Charpentier, J.P., Gharbi, H., Valès, F., 2005. Very slow creep tests on rock samples. International Journal of Rock Mechanics and Mining Sciences 42, 569–576.

Breunese, J.N., Van Eijs, R.M.H.E., De Meer, S., Kroon, I.C., 2003. Observation and Prediction of the Relation Between Salt Creep and Land Subsidence in Solution Mining—The Barradeel Case. Solution Mining Research Institute, Chester, U.K., pp. 38–57.

Campos de Orellana, A.J., 1998. Non-associated pressure solution creep in salt rock mines. In: Aubertin, M., Hardy Jr., H.R. (Eds.), The Mechanical Behaviour of Salt IV—Proceedings of the Fourth Conference Series on Rock and Soil Mechanics 22. Trans Tech Publications, Montreal, pp. 429–444.

Carter, N.L., Kronenberg, A.K., Ross, J.V., Wiltschko, D.V., 1990. Control of fluids on deformation of rocks. In: Knipe, R.J., Rutter, E.H. (Eds.), Deformation Mechanisms, Rheology and Tectonics Geological Society Special Publication 54, pp. 1–13.

De Bresser, J.H.P., Urai, J.L., Olgaard, D.L., 2005. Effect of water on the strength and microstructure of Carrara marble axially compressed at high temperature. Journal of Structural Geology 27 (2), 265–281.

De Meer, S., Spiers, C.J., Nakashima, S., 2005. Structure and diffusive properties of fluid-filled grain boundaries: an in-situ study using infrared (micro) spectroscopy. Earth and Planetary Science Letters 232 (3–4), 403–414.

Drury, M.R., Humphreys, F.J., 1988. Microstructural shear criteria associated with grain boundary sliding during ductile deformation. Journal of Structural Geology 10, 83–89.

Drury, M.R., Urai, J.L., 1990. Deformation-related recrystallization processes. Tectonophysics 172, 235–253.

Franssen, R.C.M.W., 1993. Rheology of synthetic rocksalt. PhD thesis, Utrecht University.

Franssen, R.C.M.W., Spiers, C.J., 1990. Deformation of polycrystalline salt in compression and in shear at 250–350 °C. In: Knipe, R.J., Rutter, E.H. (Eds.), Deformation Mechanisms, Rheology and Tectonics Geological Society Special Publication 54, pp. 201–213.

Guillopé, M., Poirier, J.P., 1979. Dynamic recrystallization during creep of single crystalline halite: an experimental study. Journal of Geophysical Research 84, 5557–5567.

Holness, M.B., Lewis, S., 1997. The structure of the halite–brine interface inferred from pressure and temperature variations of equilibrium dihedral angles in the halite–H_2O–CO_2 system. Geochimica et Cosmochimica Acta 61 (4), 795–804.

Hughes, D.A., Liu, Q., Chrzan, D.C., Hansen, N., 1997. Scaling of microstructural parameters: misorientations of deformation induced boundaries. Acta Materialia 45 (1), 105–112.

Hull, D., Bacon, D.J., 1984. Introduction to Dislocations. Pergamon Press, Oxford.

Humphreys, F.J., 2004. Characterization of fine-scale microstructures by electron backscattered diffraction (EBSD). Scripta Materialia 51, 771–776.

Humphreys, F.J., Hatherly, M., 1996. Recrystallization and Related Annealing Phenomena. Pergamon Press, Oxford.

Humphreys, F.J., Bate, P.S., Hurley, P.J., 2001. Orientation averaging of electron backscattered diffraction data. Journal of Microscopy 201 (1), 50–58.

Hurley, P.J., Humphreys, F., 2002. Characterizing the deformed state in Al–0.1Mg alloy using high-resolution electron backscattered diffraction. Journal of Microscopy 205 (3), 218–225.

Kronenberg, A.K., Castaing, J., Mitchell, T.E., Kirby, S.H., 2000. Hydrogen defects in α–Al_2O_3 and water weakening of sapphire and alumina ceramics between 600 and 1000 °C—I. infrared characterization of defects. Acta Materiala 48, 1481–1494.

Lebensohn, R.A., Dawson, P.R., Kern, H.M., Wenk, H.-R., 2003. Heterogeneous deformation and texture development in halite polycrystals: comparison of different modeling approaches and experimental data. Tectonophysics 370, 287–311.

Lister, G.S., Dornsiepen, U.F., 1982. Fabric transitions in the Saxony Granulite terrain. Journal of Structural Geology 4, 81–92.

Mackwell, S.J., Kohlstedt, D.L., Paterson, M.S., 1985. The role of water in the deformation of olivine single crystals. Journal of Geophysical Research 90, 11319–11333.

Martin, B., Roller, K., Stockhert, B., 1999. Low-stress pressure solution experiments on halite single-crystals. Tectonophysics 308 (3), 299–310.

McLaren, A.C., Fitz Gerald, J.D., Gerretson, J., 1989. Dislocation nucleation and multiplication in synthetic quartz: relevance to water weakening. Physics and Chemistry of Minerals 16, 465–482.

Passchier, C.W., Trouw, R.A.J., 1996. Microtectonics. Springer, Berlin.

Peach, C.J., Spiers, C.J., 1996. Influence of crystal plastic deformation on dilatancy and permeability development in synthetic salt rock. Tectonophysics 256, 101–128.

Peach, C.J., Spiers, C.J., Trimby, P.W., 2001. Effect of confining pressure on dilation, recrystallization, and flow of rock salt at 150 °C. Journal of Geophysical Research 106 (B7), 13315–13328.

Pennock, G.M., Drury, M.R., 2005. Low angle subgrain misorientations in deformed NaCl. Journal of Microscopy 217, 130–137.

Pennock, G.M., Drury, M.R., Trimby, P.W., Spiers, C.J., 2002. Misorientation in hot deformed NaCl using EBSD. Journal of Microscopy 205, 285–294.

Pennock, G.M., Drury, M.R., Spiers, C.J., 2004. Investigation of subgrain rotation recrystallization in dry polycrystalline NaCl. Materials Science Forum 467–470, 597–602.

Pennock, G.M., Drury, M.R., Spiers, C.J., 2005. The development of subgrain misorientations with strain in dry synthetic NaCl measured using EBSD. Journal of Structural Geology 27 (12), 2159–2170.

Randle, V., 1992. Microtexture Determination and its Application. Institute of Materials, London.

Read, H.H., Watson, J., 1969. Introduction to Geology, Volume 1 Principles. Macmillan, London.

Ree, J.-H., 1994. Grain boundary sliding development of grain boundary openings in experimentally deformed octachloropropane. Journal of Structural Geology 16 (3), 403–418.

Rutter, E.H., 1972. The influence of interstitial water on the rheological behaviour of calcite rocks. Tectonophysics 14 (1), 13–33.

Sakai, T., Jonas, J.J., 1984. Dynamic recrystallization: mechanical and microstructural considerations. Acta Metallurgica 32 (2), 189–209.

Schmid, S.M., Paterson, M.S., Boland, J.N., 1980. High temperature flow and dynamic recrystallization in Carrara marble. Tectonophysics 65, 245–280.

Shenk, O., Urai, J.L., 2004. Microstructural evolution and grain boundary structure during static recrystallization in synthetic polycrystals of sodium chloride containing brine. Contributions to Mineral Petrology 146, 671–682.

Singh, V., Rao, P.R., Taplin, D.M.R., 1973. On the role of grain–boundary migration during creep of zinc. Journal of Material Science 8, 373–381.

Skrotzki, W., 1994. Mechanism of texture development in rocks. In: Bunge, H.J., Siegesmund, S., Skrotski, W., Weber, K. (Eds.), Textures of Geological Materials. DGM Verlag, Göttingen, Germany, pp. 167–186.

Skrotzki, W., Welch, P., 1983. Development of texture and microstructure in extruded ionic polycrystalline aggregates. Tectonophysics 99, 47–61.

Spiers, C.J., Brzesowsky, R.H., 1993. Densification behaviour of wet granular salt: theory versus experiment. In: Seventh Symposium on Salt 1, Elsevier, Amsterdam, pp. 83–92.

Spiers, C.J., Urai, J.L., Lister, G.S., Boland, J.N., Zwart, H.J., 1986. The influence of rock–fluid interaction on the rheological and transport properties of dry and wet salt rocks. European Communities—Commission, Nuclear Science and Technology Series. EUR-10399.

Spiers, C.J., Schutjens, P.M.T.M., Brzesowsky, R.H., Peach, C.J., Liezenberg, J.L., Zwart, H.J., 1990. Experimental determination of constitutive parameters governing creep of rocksalt by pressure solution. In: Knipe, R.J., Rutter, E.H. (Eds.), Deformation Mechanisms, Rheology and Tectonics Geological Society Special Publication 54, pp. 215–227.

Stokes, R.J., 1966. Mechanical properties of polycrystalline sodium chloride. Proceedings of the British Ceramic Society 6, 189–207.

Ter Heege, J.H., 2002. Relationship between dynamic recrystallization, grain size distribution and rheology. PhD Thesis, Utrecht University.

Ter Heege, J.H., De Bresser, J.H.P., Spiers, C.J., 2005a. Dynamic recrystallization of wet synthetic polycrystalline halite: dependence of grain size distribution on flow stress, temperature and strain. Tectonophysics 396, 35–57.

Ter Heege, J.H., De Bresser, J.H.P., Spiers, C.J., 2005b. Rheological behaviour of synthetic rocksalt: the interplay between water, dynamic recrystallization and deformation mechanisms. Journal of Structural Geology 27, 948–963.

Trimby, P.W., Drury, M.R., Spiers, C.J., 2000a. Misorientations across etched boundaries in deformed rocksalt: a study using electron backscattered diffraction. Journal of Structural Geology 22, 81–89.

Trimby, P.W., Drury, M.R., Spiers, C.J., 2000b. Recognising the crystallographic signature of recrystallization processes in deformed rocks: a study of experimentally deformed rocksalt. Journal of Structural Geology 22 (11-12), 1609–1620.

Urai, J.L., 1983. Water assisted dynamic recrystallization and weakening in polycrystalline bischovite. Tectonophysics 96, 125–157.

Urai, J.L., 1987. Development of microstructure during deformation of carnalite and bischofite in transmitted light. Tectonophysics 135, 251–263.

Urai, J.L., Spiers, C.J., Peach, C.J., Franssen, R.C.M.W., Liezenberg, J.L., 1987. Deformation mechanisms operating in naturally deformed halite rocks as deduced from microstructural investigations. Geologie en Mijnbouw 66, 165–176.

Urai, J.L., Spiers, C.J., Zwart, H.J., Lister, G.S., 1986. Weakening of rock salt by water during long-term creep. Nature 324, 554–557.

Watanabe, T., Peach, C.J., 2002. Electrical impedance measurement of plastically deforming halite rocks at 125 °C and 50 MPa. Journal of Geophysical Research 107 (B1), 1–12.

Wenk, H.-R., Canova, G., Brechet, Y., Flandin, L., 1997. A deformation-based model for recrystallization of anisotropic materials. Acta Materiala 45 (8), 3283–3296.

White, S.H., 1977. Geological significance of recovery and recrystallization processes in quartzites. Tectonophysics 39, 143–170.